



Performance assessment of hybrid GFRP-steel reinforced concrete shear walls under in-plane cyclic loads

Hesham Haggag¹ Hany el-Kady¹ Osama Amer^{2,*}, Ahmed H. Ali²,

¹Department of Civil Engineering, Faculty of Engineering, Helwan University, Cairo, Egypt

²Department of Civil Engineering, Faculty of Engineering, Ain Shams University, Cairo, Egypt.

*Corresponding Author E-mail: osama_amer@cu.edu.eg

الملخص العربي :

يعد استخدام قضبان الصلب في تسليح الأجزاء الخرسانية عرضة للتآكل الذي يؤثر على الأداء العام والمتانة خاصة للعناصر الخرسانية المعرضة لبيئة عدوانية. حديثاً، تستخدم قضبان البوليمرات المقوى بالألياف الزجاجية كتسليح بديل للعناصر الخرسانية وذلك نظراً لمقاومتها للتآكل إضافة الى ارتفاع مقاومتها لإجهادات الشد العالية نسبة الى وزنها. بالرغم من ذلك، القليل من الدراسات السابقة تناولت استخدام قضبان البوليمرات المقواه بالألياف الزجاجية لتقوية جدران القص الخرسانية. يتناول هذا البحث دراسة أداء جدران القص المسلحة باسياخ الصلب، وقضبان البوليمرات المقوى بالألياف الزجاجية ، وايضاً نظام تسليح هجين يدمج بين استخدام قضبان الصلب وقضبان البوليمرات المقواه بالألياف الزجاجية تحت تأثير الأحمال الدورية الجانبية. وقد تم اقتراح واختبار التسليح الهجين الذي يدمج بين قضبان الصلب والبوليمرات المقواه بالألياف الزجاجية لإجراء فحص شامل لقدرة هذا النظام على تسليح جدران القص الخرسانية المسلحة في المباني المتوسطة الارتفاع

الكلمات المفتاحية : حوائط القص، الخرسانة المسلحة، السلوك الإنشائي، الأحمال الديناميكية

ABSTRACT :

The use of steel bars for reinforcement of concrete members is vulnerable to corrosion which affect on the overall performance and durability of concrete elements subjected to aggressive environment. Glass-Fibre-Reinforced-Polymer (GFRP) bars are used as alternative reinforcement for their corrosion resistance and high tensile-to-weight ratio. In addition, the use of GFRP bars to reinforce concrete shear walls is rarely. This paper investigates the performance of shear walls reinforced with steel, GFRP, and even a combination of them (hybrid steel-GFRP) under lateral cyclic loading. Six RC shear walls reinforced with steel and GFRP bars were tested under pseudo-static reversed-cyclic lateral load. Three shear walls were reinforced by GFRP bars as longitudinal and transversal reinforcement, and two walls were reinforced with hybrid GFRP-steel bars with different ratios of web reinforcement. A reference specimen, reinforced by ordinary steel bars, was also introduced to certify the capability of GFRP as reinforcement bars. The results indicated that the GFRP-reinforced concrete slender walls had a stable hysteretic response and small residual drift up to failure. Higher displacement capacity, increased lateral

strength and equivalent viscous damping coefficient were observed with the increase of GFRP web reinforcement ratio. Moreover, the fundamental period of GFRP and hybrid GFRP-steel reinforced walls can reach more than twice its original value prior to failure. The hybrid steel-GFRP reinforcement was proposed and tested to thoroughly investigate the capability of this system for reinforced concrete shear walls in mid-rise buildings. The GFRP bars were used to achieve stable resistance capacity and small residual deformation, thus eliminating the steel corrosion problem and consequently providing more safety to RC shear wall structures and reducing their maintenance cost. Moreover, the effects of the GFRP web reinforcement ratio on different behavioural aspects are also investigated, and the results quantify the strength and deformability characteristics of Hybrid GFRP-steel reinforcement walls.

KEYWORDS: Hysteretic behaviour, Reinforced concrete, Shear walls, Seismic behavior

1. INTRODUCTION

The use of reinforced concrete (RC) walls is frequently recommended as a reliable bracing solution with promising performance for lateral load resistance and drift control in mid-and-high-rise buildings. This fact was experimentally confirmed in literature as RC shear walls offered high lateral strength, stiffness, and deformation capacity under seismic loading. Therefore, it is essential to understand the actual behaviour of RC shear walls and its seismic performance in order to appropriately analyse their failure mechanisms and create more dependable and cost-effective designs, knowing that the performance-based design techniques are increasingly frequently used for new structures [1-3].

A shear strength failure criterion for shear walls was established in earlier investigations [4]. In the study, a database of previous testing on minimally reinforced shear walls was put together and examined. The findings showed that the quantity of boundary reinforcement provided, the existence of axial load, and the position of a weak plane joint on the wall were the most significant elements that affect the nominal shear strength. Oh et al. [5] studied the effect of boundary element details, confinement, and end configurations of RC structural walls on their deformation capacities. The study included testing Four full-scale wall specimens (three rectangular and a barbell-shaped cross-section wall) having different transverse reinforcement content at the boundaries. The authors concluded that the barbell and the well-confined rectangular wall showed similar deformation capacities, drift ratio and energy dissipation. Beyer et al. [2], tested half-scaled U-Shaped/channel-shaped structural walls to evaluate their flexural behaviour in different loading directions. The tests indicated that the most critical direction was the diagonal loading direction, where the displacement capacity was the smallest. Preti and Giuriani [6] investigated the ductility of the reinforced concrete structural walls in buildings of mid-rise height. In this study, a full-scale five-story RC wall was tested. The wall was reinforced with unusual large rebar diameters uniformly distributed along the wall length. High ductility capacity was attained for the tested wall, ensuring a uniform crack pattern and

eliminating any premature web rebar fracture, shear sliding, and crack localisation in the web region.

According to experimental findings in the literature, the behaviour of shear walls is primarily depended on the geometric characteristics of the walls; for squat walls ($\alpha_s = h_w/l_w \leq 2$) the response is governed by shear, while the response of slender walls ($\alpha_s \geq 2$) is dominated by flexural [1,4,7]. This study focuses on slender shear walls, commonly used for mid- and high-rise buildings. They are usually designed to resist lateral loads primarily through flexural behaviour and to withstand significant inelastic flexural deformations prior to strength loss, i.e., ductile behaviour.

The selection of reinforcement is one of the most crucial factors to be considered when designing reinforced concrete (RC) structures. Despite the fact that conventional steel has long been the most common type of reinforcement for concrete structures, its susceptibility to corrosion presents a significant problem for buildings located in harsh climates. Steel corrosion causes the effective cross-section of the reinforcing bars to decrease drastically, eventually resulting in unexpected failures. Corrosion causes a reinforcing steel bar's volume to increase by up to three times its initial size. Additionally, the surrounding concrete might also spall and crack as a result of that expansion [3]. Conversely, GFRP reinforcing bars are inherently immune to corrosion, which offers a desirable alternative to conventional steel reinforcement for reinforced concrete structures, including columns, beams, and one-way and two-way slabs [8-13].

The interest in using Glass fibre reinforced polymer (GFRP) bars lies within their resistance to corrosion of the reinforced concrete structures where climatic condition is aggressive [14, 15]. Besides high corrosion resistance, GFRP bars in reinforced concrete structures have shown advantages such as a higher tensile strength-to-weight ratio than steel reinforcement and their ability to conform to uneven surfaces. However, there are still few applications of FRP, and its use is not widespread. Lack of design knowledge among practising engineers is one of the primary challenges facing the designer of FRP-reinforced concrete elements. The nearly elastic stress-strain response of FRP reinforcing materials is another limitation since it precludes their application in areas prone to seismic events where ductility and nonlinear behaviour are desired [3]. Thus, the purpose of this research is to determine whether GFRP bars could be used as a primary reinforcing element or as part of a hybrid GFRP-steel reinforcement for reinforced concrete shear walls. The main objective is to better understand the failure mechanisms of GFRP-RC shear walls by evaluating its behaviour and response under in-plane cyclic loads. This study focused on the seismic performance of slender (flexural controlled) shear walls, as they are commonly used in mid-to high-rise buildings. Although the current study considered only one type of FRP reinforcement, GFRP, the results can still be easily implemented in other FRP types.

2. Material and methods

2.1. Wall Specimens

Six RC shear walls were tested as part of the experimental programme under quasistatic cyclic loading till failure. The tested walls included three GFRP-reinforced specimens (GW1, GW2, and GW3), one reference steel-reinforced specimen (SW1), and two walls

with hybrid GFRP-steel reinforcement. The minimum thickness and reinforcement details were designed according to [16] for the steel-reinforced wall and [17] for the GFRP-reinforced walls. Plane sectional analysis was adopted to predict the ultimate lateral load (Figure 3), assuming the concrete compressive strain (ε_{cu}) limit equals 0.003. Internal force equilibrium (Eq. 1) and strain compatibility relationship (Eq. 2) formed the bases for the utilized plane-sectional analysis [18]; consequently, the flexural strength of the RC wall was determined.

$$M_i = C_c \left(c - \frac{\alpha}{2} \right) + \sum_1^n A_{si} f_{si} (c - X_i) + P_i \left(\frac{l_w}{2} - c \right) \quad \text{Eq. 1}$$

$$\varepsilon_{si} = \varepsilon_{cu} \frac{c - X_i}{c} \quad \text{Eq. 2}$$

The theoretical shear strength (V_r) was determined using sectional shear-analysis equations as the sum of the concrete shear strength (V_c) and the shear strength (V_f) provided by horizontal web reinforcement [19], as shown in Eq. 3-5.

$$V_r = V_c + V_f \quad \text{Eq. 3}$$

$$V_c = \frac{2}{5} \sqrt{f'_c} b_w (k d) \quad \text{Eq. 4}$$

$$V_f = \frac{A_f v f_f v d}{s} \quad \text{Eq. 5}$$

The tested walls were designed with adequate reinforcement to ensure flexural domination and prevent sliding shear and anchorage failures. Moreover, two layers of vertical reinforcements were provided for all walls to limit the potential out-of-plane displacement and increase the walls' stability [20, 21], as shown in Table 1. Figure 4 presents the concrete dimension and reinforcement details of the tested walls.

Table 1 - Details of the wall specimens

Specimens		Vertical reinforcement (%)			Horizontal reinforcement			Predicted capacity (kN)
		No. & size	$\rho_{v,s}$	$\rho_{v,f}$	No. & size	$\rho_{h,s}$	$\rho_{h,f}$	
Steel-Reinforced wall	SW Control	10 T12 ^a	0.71	-	T8 ^b @ 125 mm	0.40	-	86.00
Hybrid GFRP-steel reinforced walls	SGW1	4 T12 + 6F4 ^c	0.28	0.48	F3@ 125 mm	-	1.01	97.64
	SGW2	6 T12 + 10F4	0.42	0.79	F3@ 125 mm	-	1.01	93.17
GFRP-reinforced wall	GW1	10F4	-	0.79	F3@ 125 mm	-	1.01	133.83
	GW2	16F4	-	1.27	F3@ 125 mm	-	1.01	140.85
	GW3	22F4	-	1.74	F3@ 125 mm	-	1.01	174.75

^aSteel bars $d_b = 12mm$; ^bSteel bars $d_b = 8mm$; ^cGFRP bars No. 4.

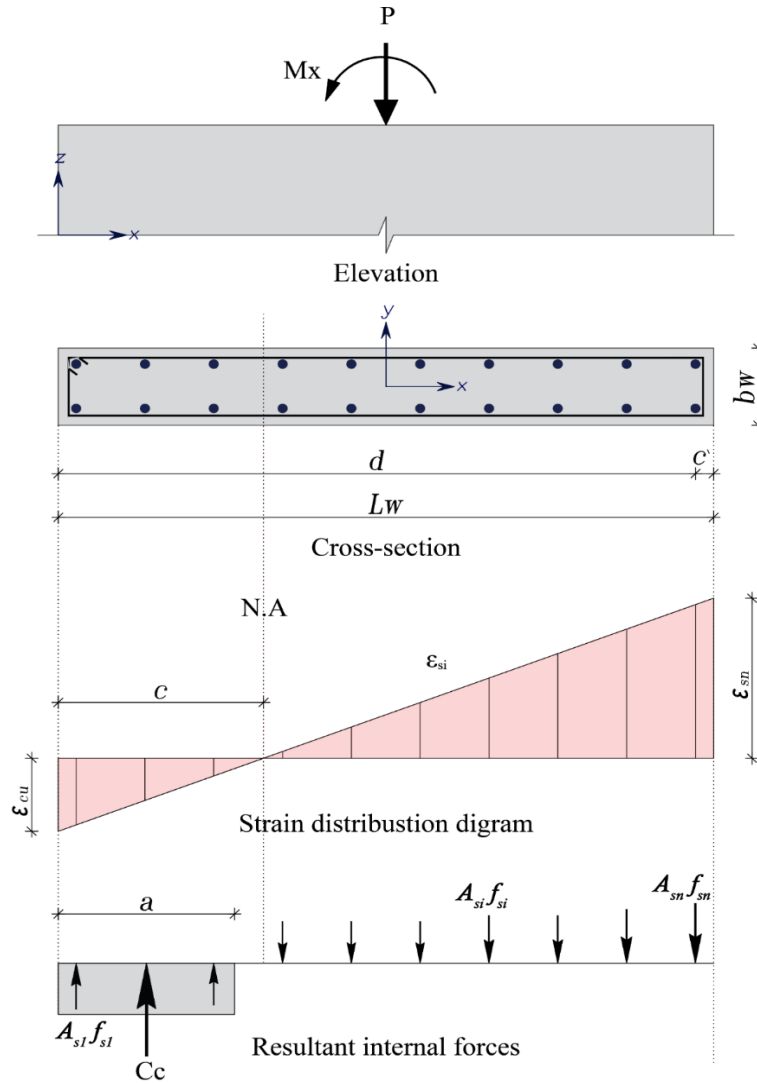


Figure 3 – Force equilibrium and strain distribution in wall cross-sections

2.2. Materials

All specimens were constructed using normal-weight and ready-mixed concrete with a targeted concrete compressive strength (f'_c) of 30 MPa. Three concrete cylinders with 150mm diameter and 300mm height were prepared from each pour and tested under compression following [22]. For steel reinforcement, 8mm Grade 240/350 steel bars were used for horizontal reinforcement and 12mm Grade 400/600 steel bars were used for vertical reinforcement. Moreover, #4 sand-coated straight GFRP reinforcing bars were used for the horizontal and vertical reinforcement ($f_{fu} = 1392\text{MPa}$, $E_f = 69.6\text{GPa}$, $\epsilon_{fu} = 2\%$, $A_f = 126.7\text{mm}^2$). U-shaped steel bars of 8mm diameter were used at both ends of the GFRP-reinforced walls to avoid the bent proportion of GFRP bars (Figure 5).

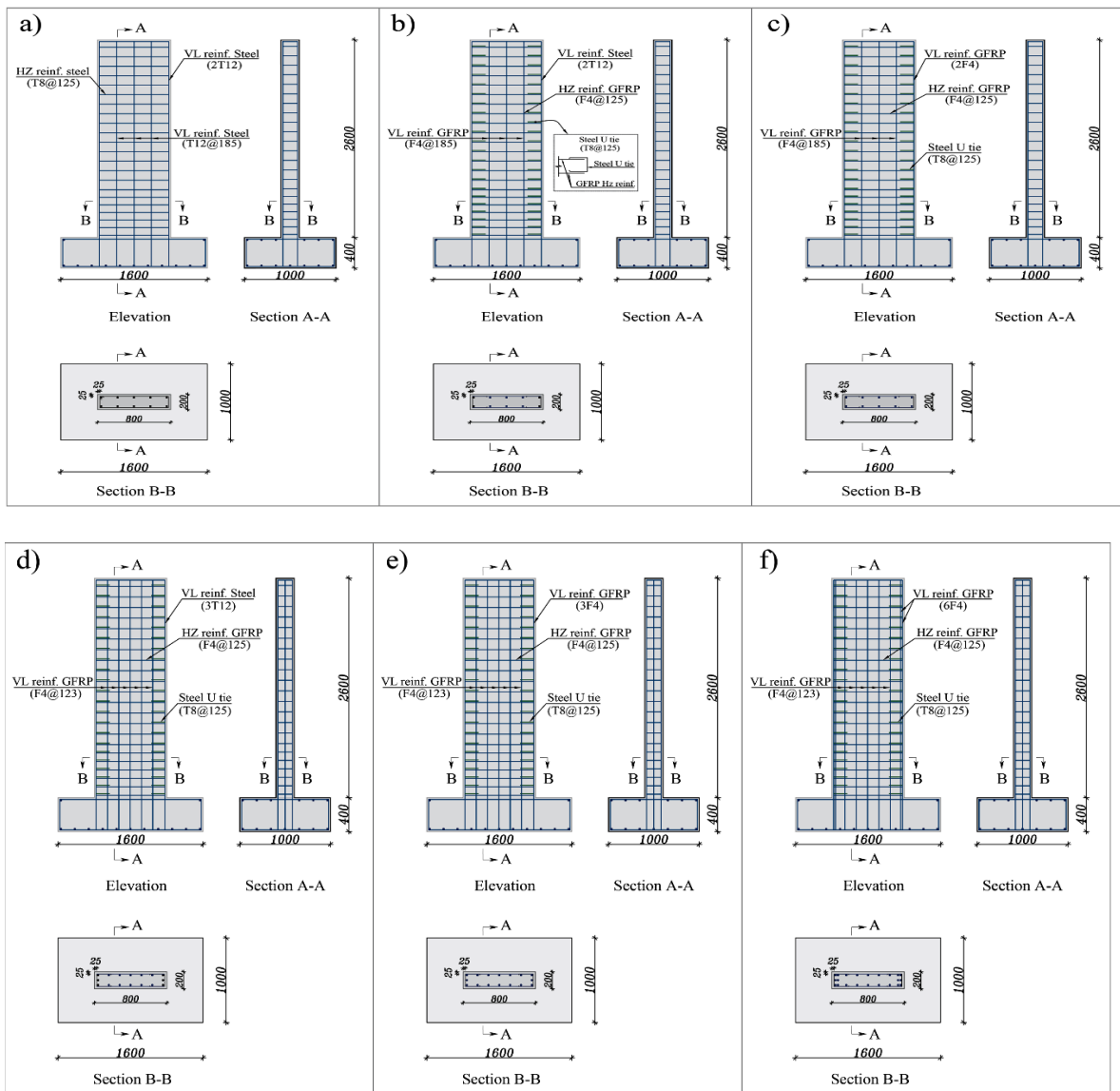


Figure 4 – Concrete dimensions and details of reinforcement configuration of walls (a) SW1 (b) SGW1, (c) GW1, (d) SGW2, (e) GW2, and (f) GW3. All dimensions in mm

2.3. Testing and instrumentation

A lateral reverse-cyclic load was applied at the top of the walls using a displacement-controlled hydraulic actuator with a maximum stroke of ± 250 mm while restraining any potential horizontal movement at the base and the vertical movement of each tested wall. No axial load (other than self-weight) was applied to walls during testing. Five LVDTs were used to measure and record the vertical and lateral displacements at various points. Strain gauges were attached to the two outermost vertical reinforcement bars 100 mm above the interface between the wall and the foundation. The horizontal deflection was measured at the top of each wall to control the displacement protocol. The wall specimen was positioned between two reaction steel frames, and a specially fabricated load transfer

system was fixed on the wall's top height, consisting of steel-plated and high-strength steel rods. The lateral load was applied at the steel girder using a 500 kN hydraulic actuator, which was fixed to the strong reaction frame and the load-transfer system of the walls, as shown in Figure 6. The imposed lateral loading protocol comprised two fully-reversed lateral drift cycles (Figure 6b) applied at gradually increasing drift levels as per FEMA 461-07 [23].

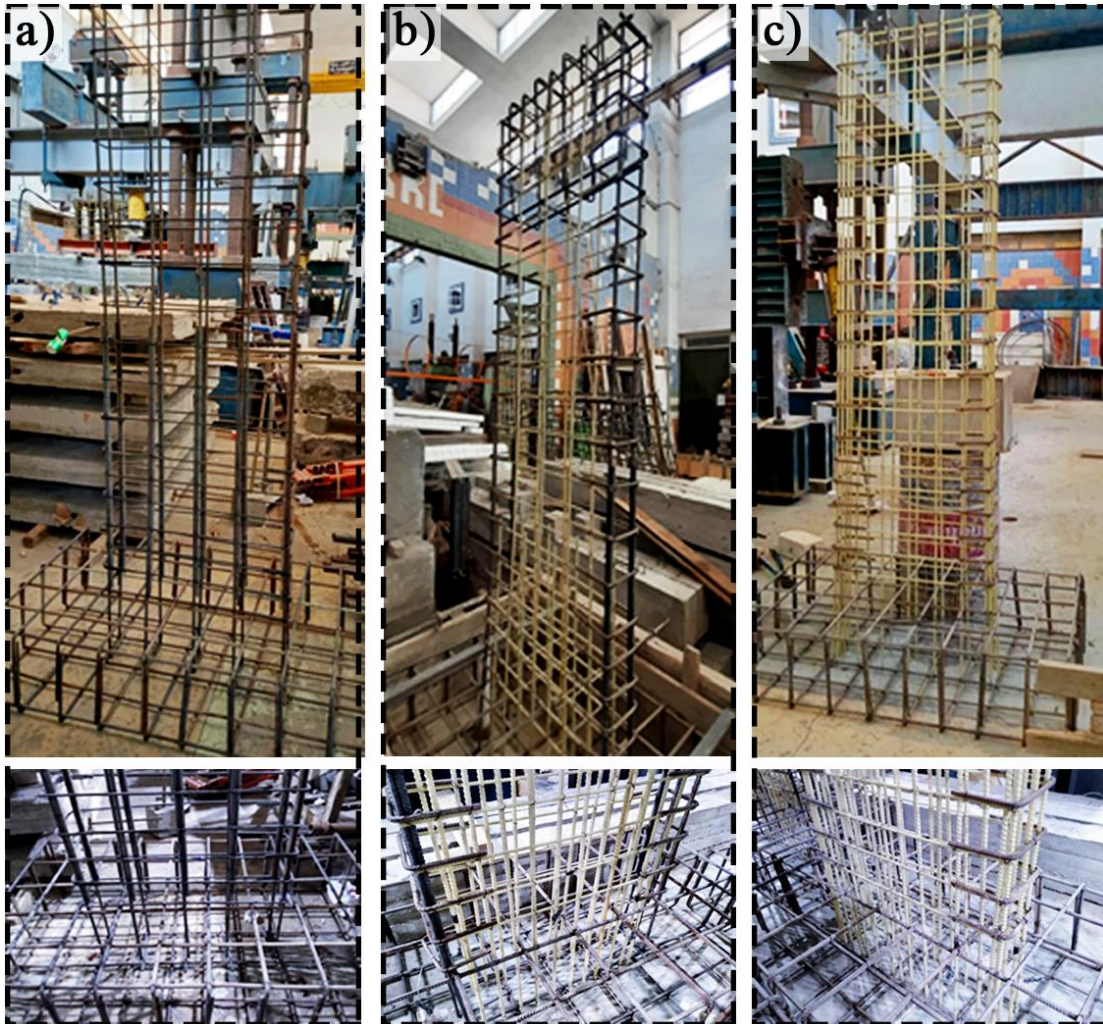


Figure 5 – Reinforcement configuration of (a) steel, (b) hybrid steel-GFRP, and (c) GFRP reinforced walls

3. Main test results

3.1. Displacement Response History

The shear wall's seismic performance significantly depends on the force versus displacement relationship. Continuous plots of applied force versus displacement hysteresis relationships and envelope curves of all tested walls were recorded and plotted in Figure 7-7. In each graph, the vertical, ρ_v , and horizontal, ρ_h , reinforcement ratios are shown. The top right quadrant shows the load-displacement relationships in the push (+) direction, and vice versa for the bottom left quadrant that plots the load-displacement

relationships in the pull (–) direction. The primary axes plot the lateral force (F) acting on the wall versus the top displacement (Δ) obtained from the recorded displacement from the top horizontal LVDT. The secondary axes of the presented graphs display the drift (δ) versus load multiplier (λ). The load multiplier (non-dimensional load format) is defined as the ratio of the wall’s lateral force resistance to its self-weight $\lambda = \frac{Q}{W_{wf}}$.

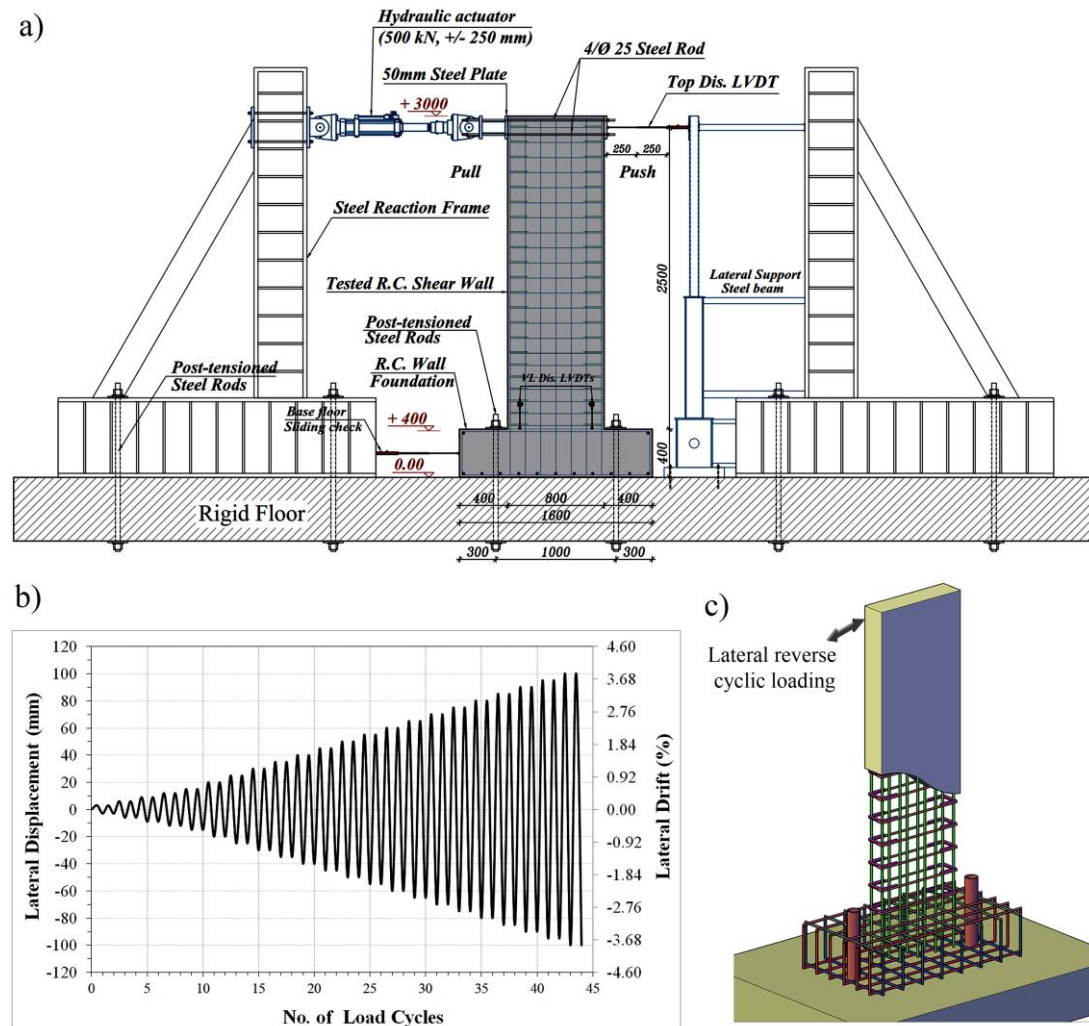


Figure 6 – Layout of the test setup and used LVDTs (a), Applied displacement-controlled loading history (b) and (c) schematic 3d view of the tested walls

Overall, the hysteretic response of the tested walls appears to be self-centring and showed reasonably stable lateral load-displacement relationships. The behaviour in the push and pull loading directions was almost symmetric, with no significant load or displacement residuals over a large part of the test until concrete crushing occurred at one end. For steel-reinforced and hybrid steel-GFRP reinforced walls (SW and SGW), the performance of the specimens was initially elastic, followed by an inelastic behaviour with gradual degradation in stiffness until the failure occurred. The hysteretic curves presented thin and slender loops upon the yielding of the outmost steel bars, indicating initially stiff behaviour and a lower level of damage. The slope of the curve decreased in each loading

cycle beyond the initial uncracked stage. With the subsequent cycling of the wall, the slope of the curve further degraded into relatively wider loops of higher displacement levels

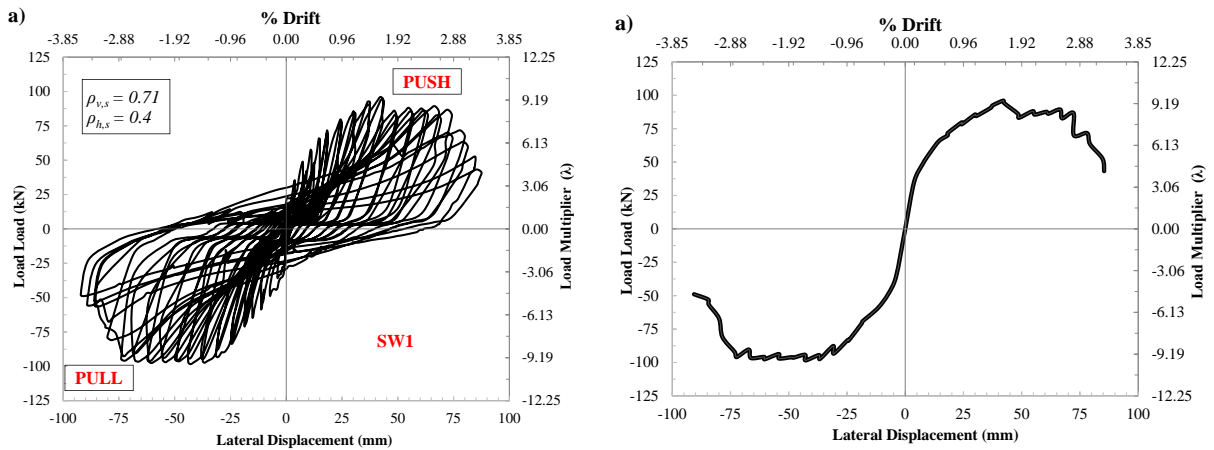


Figure 7 – Hysteretic load-displacement response of steel reinforced wall (SW1)

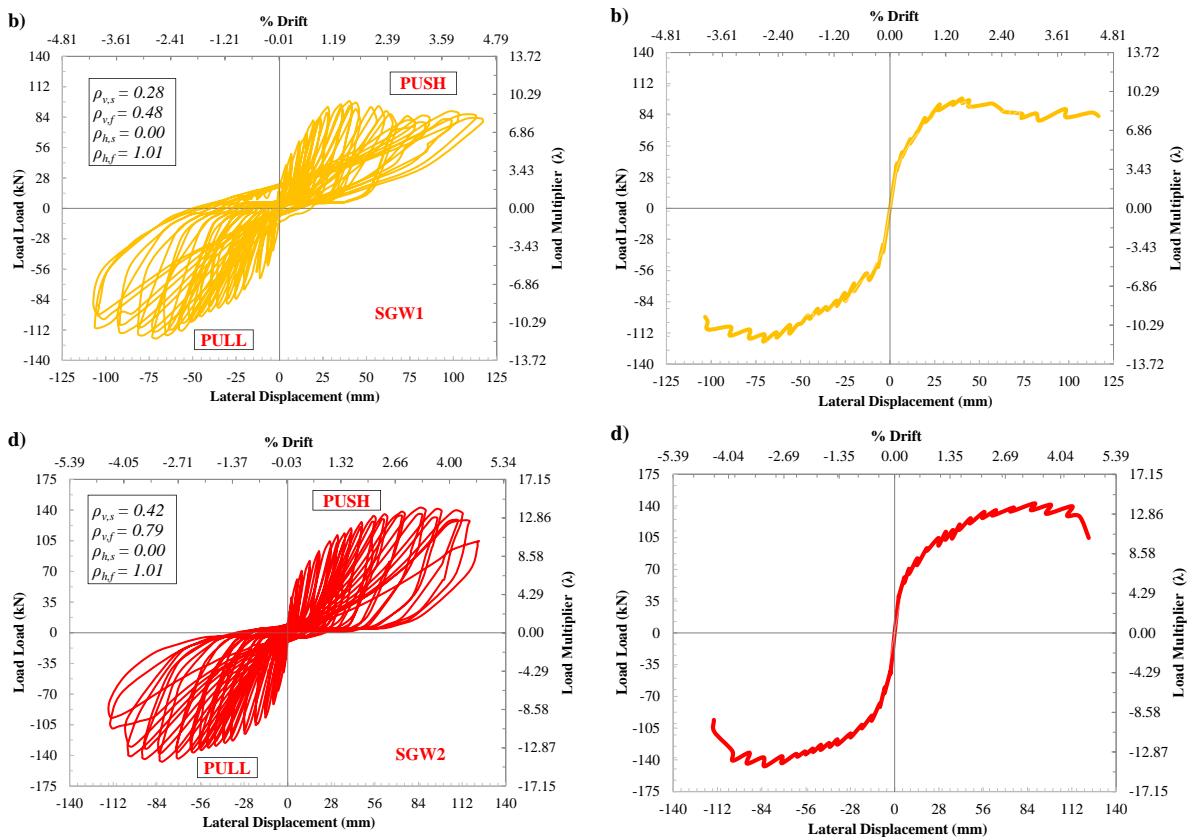


Figure 8 – Hysteretic load-displacement response of hybrid steel-GFRP reinforced walls (SGW1 and SGW2). Further opening of the loops indicates a higher damage level, which would increase energy dissipation capabilities. Contrarily, the GFRP reinforcement's elastic behaviour and the lack of yielding led to a continuously increasing gain in strength up to failure, with no strength degradation within a reasonable range of deformations. The loading, unloading, and reloading curves demonstrated linear behaviour with narrower hysteresis loops than

the corresponding steel-reinforced walls following the elastic behaviour of GFRP bars. The behaviour was almost symmetric up to failure in both push and pull loading directions, resulting in a pinched hysteresis response without any reduction of overall strength. This stable hysteresis loop behaviour is typical of a response that is flexural-dominated.

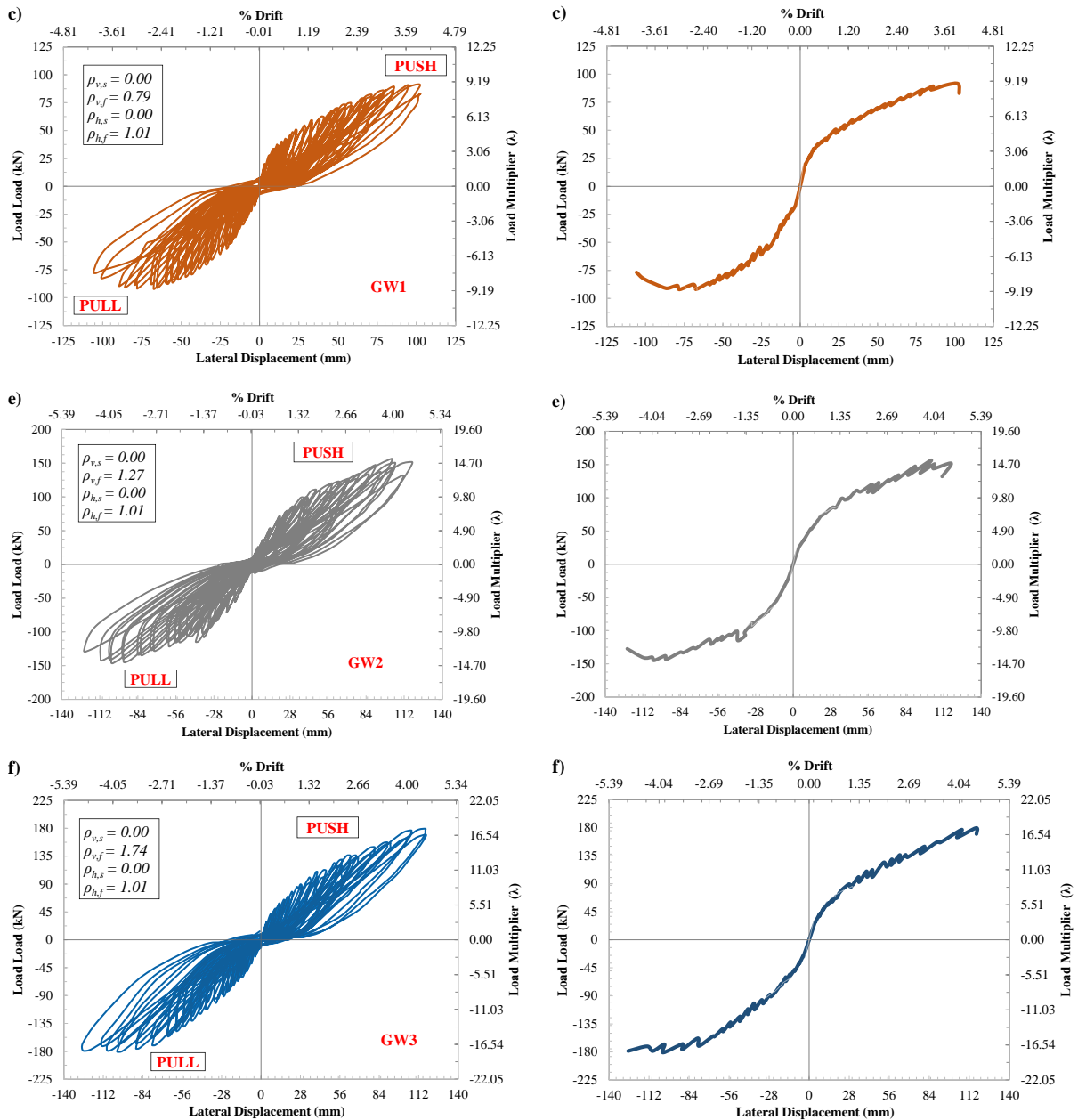


Figure 9 – Hysteretic load-displacement response of GFRP-reinforced walls (GW1, GW2 and GW3)

3.2. Failure modes and extent of damage

In general, the behaviour of all walls was dominated by a flexural response. However, crack patterns differed during loading cycles due to different reinforcement types and ratios. The specimens exhibited nearly linear behaviour before cracking. Almost a similar strength level corresponding to the crack initiation was attained for all tested walls, as it mainly depends on the concrete compressive strength. The first horizontal flexural crack

for all the tested walls was initiated at the bottom of all walls at an average drift level of 0.22%. Likewise, the concrete-cover splitting at the wall edge was recorded at almost similar drift levels ranging between 0.7% and 0.83%, where the concrete compressive strain exceeded 0.003. The cracks developed in succession from the bottom of the wall up to a height of approximately $(\frac{2}{3})h_w$ and were accompanied by diagonal shear flexural cracking of the web without any premature shear or anchorage failure. The failure mode for all walls was characterized by horizontal cracking and concrete spalling, followed by the formation of flexural cracks at the base cross-section as a result of the growing bending moment. More significant spalling of the concrete cover at the compression end of the wall is attained with increasing displacement accompanied by buckling/rupture of the outermost vertical reinforcement bars and crushing of the concrete at the toes. The failure of steel-reinforced and hybrid steel-GFRP-RC walls followed a remarkably similar pattern, characterized by local buckling of outmost longitudinal steel bars and crushing of concrete at the toe of the walls.

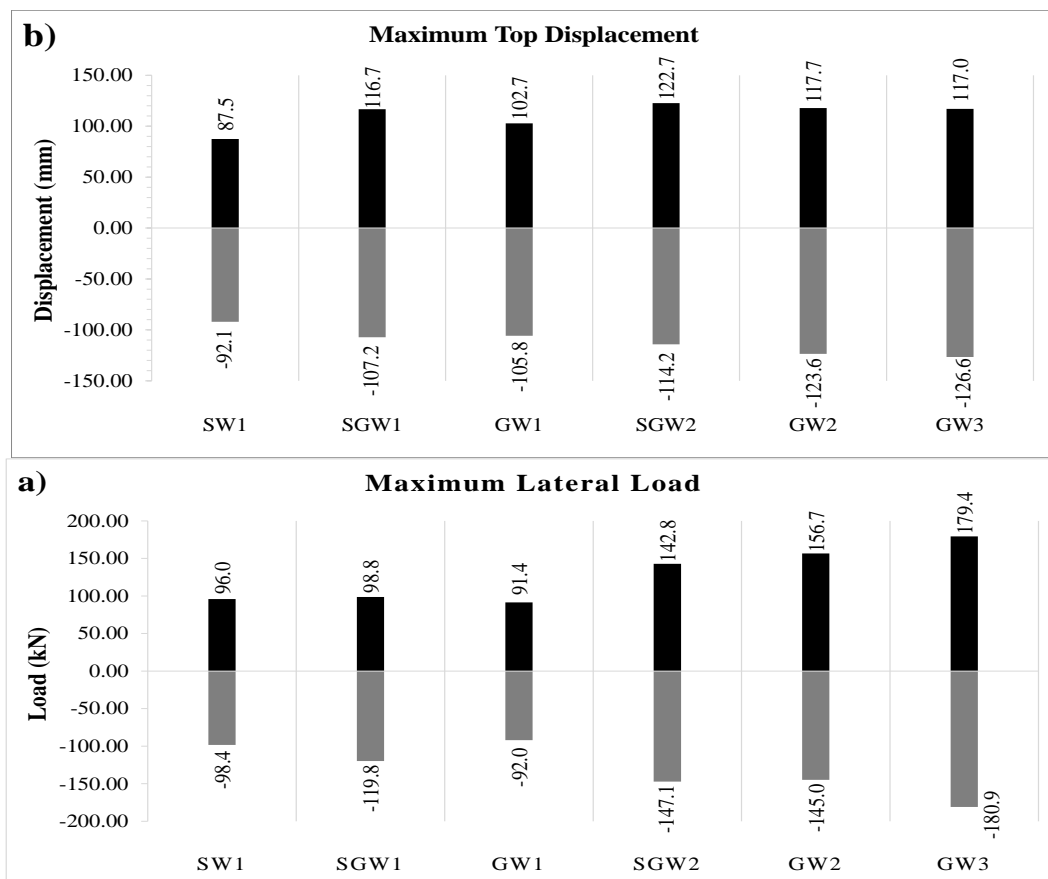


Figure 10 – Comparison between the maximum recorded loads (a) and displacement (b) of all tested walls

However, hybrid specimens featured fewer residual drift ratios than the control wall (SW1). The GFRP-reinforced walls exhibited notable linear behaviour up to its ultimate strength, where the failure stage started at the peak load and lasted until the test's end. Concrete cover splitting was gradually initiated at the outmost heavily compressed wall toe. As loading continued, the walls continued to carry the load in each cycle with no strength degradation until concrete crushing and fracture of the longitudinal GFRP bars occurred, which caused wall brittle failure without a considerable decrease in the recorded walls' strength. Further, higher GFRP-reinforcement ratios resulted in higher crack propagation and brittle failure. A combined shear-flexure failure mechanism was only observed in walls GW2 and GW3, where sliding shear deformations are developed after maximum strength due to the web's diagonal cracking. The performance parameters recorded at the primary damage levels are summarized in Figure 11. The final crack patterns and typical failure modes of the specimens are shown in Figure 12. Close-up photos of the major damage aspects are presented in Figure 13.

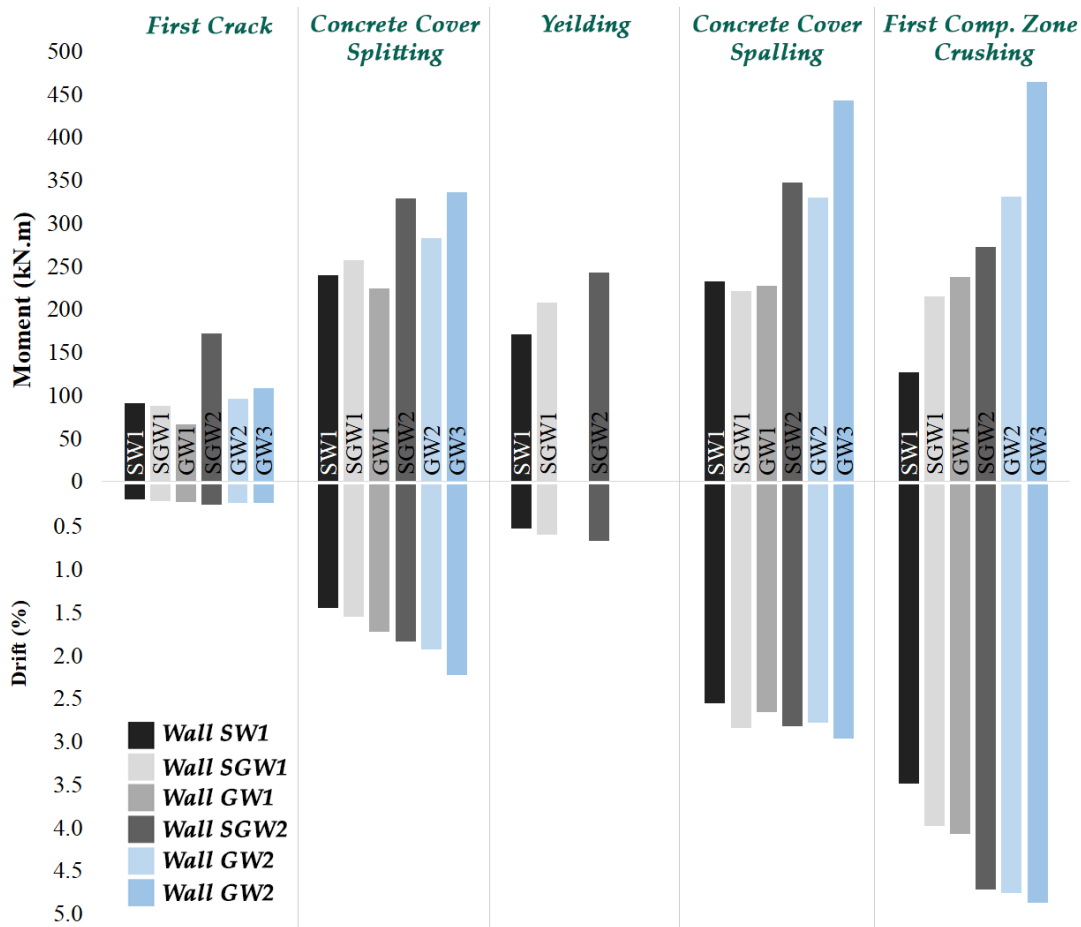


Figure 11 – Summary of damage propagation for all tested walls

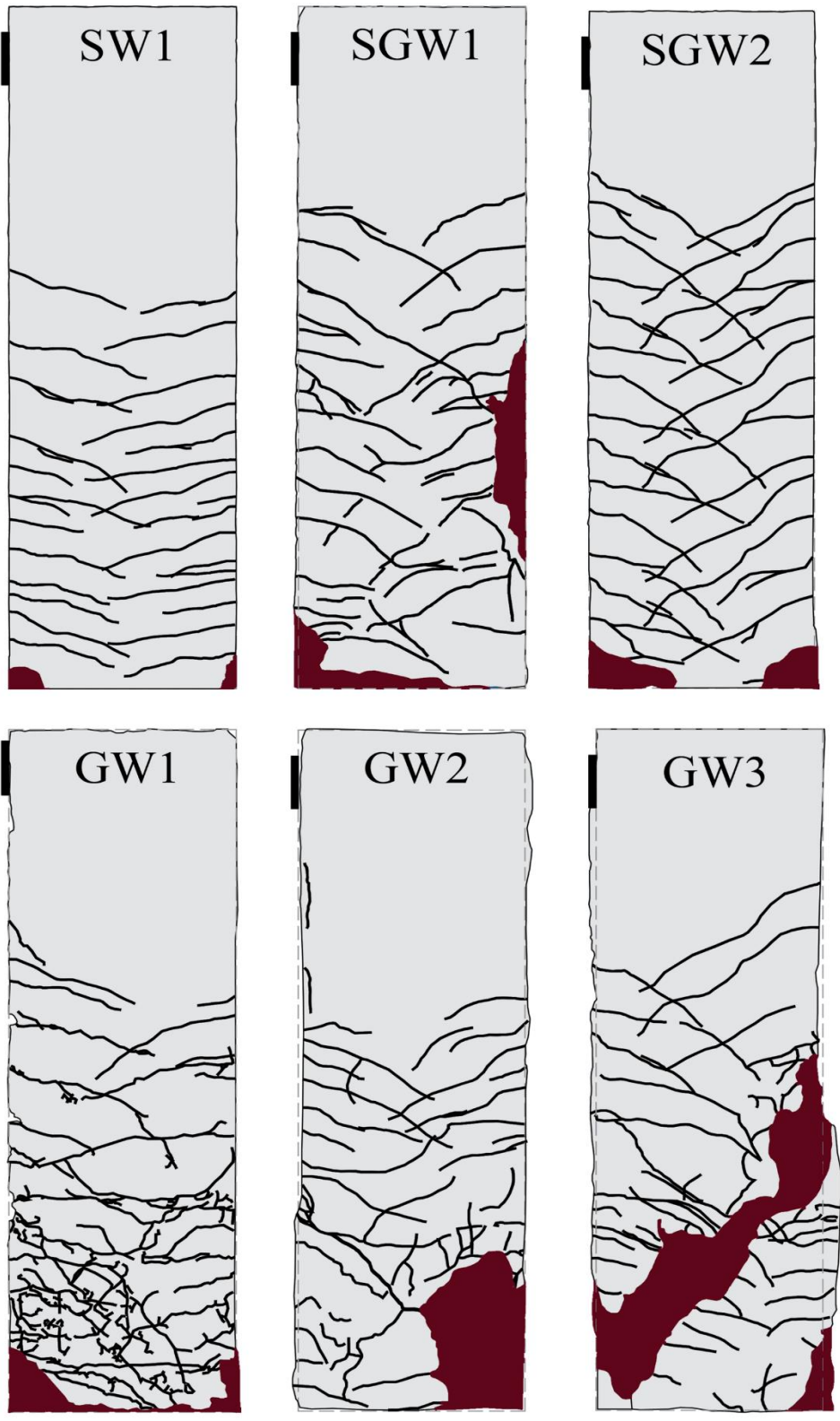


Figure 12 – Observed crack patterns prior to failure

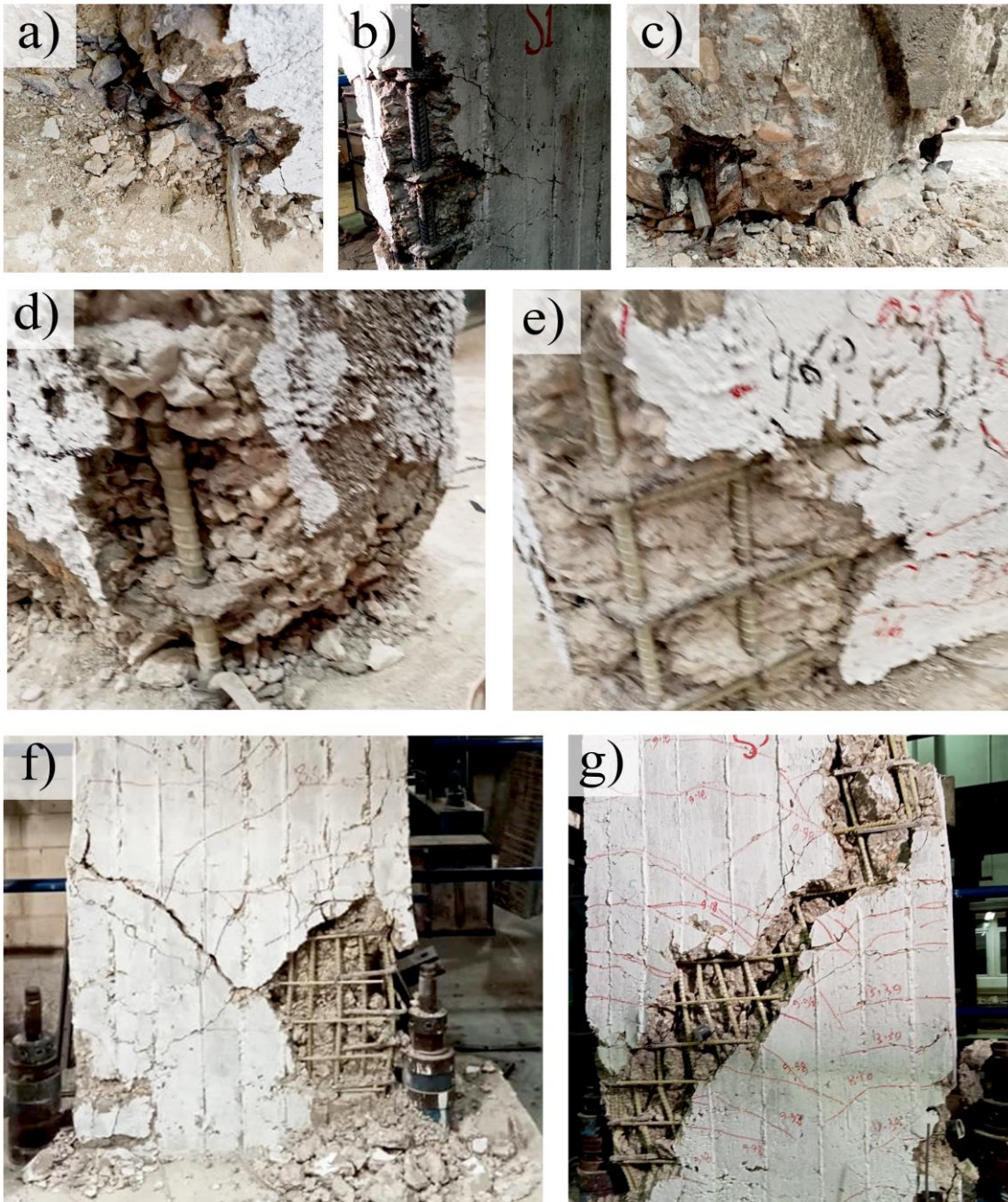


Figure 13 – Close-up photos for the major damage states

4. Characteristic experimental behaviour

4.1. Self-centering behaviour

The recovered drift ratio over the maximum drift at different levels of drift ratio demands was used to measure the self-centring capabilities of the tested shear walls. Figure 14 and 13 illustrate the residual drift ratio of the steel-reinforced wall (SW1-control wall) during

testing. As cyclic loading progressed and higher drift ratios were applied to the walls, they sustained further residual drift ratios in a different value depending on the reinforcement type and ratio. As can be seen in Figure 15a-b, the drift ratio recovery was higher in hybrid steel-GFRP reinforced walls (SGW1 and SGW2) than in control walls. Moreover, GFRP-reinforced walls exhibited smaller residual drifts than their corresponding control walls. Furthermore, the highest drift ratio recoveries occurred in wall GW3, which had the highest GFRP reinforcement ratio. The recovery in the residual drift ratio of each hybrid specimen with respect to the control wall is shown in Figure 15f. According to the obtained results, the maximum self-centring of the slender hybrid wall was observed at 3.6% drift, where the residual drift ratios of the walls SGW1 and SGW2 were 46.5% and 58.3%, respectively, smaller than the steel-reinforced wall. The higher reduction ratio for wall SGW2 compared to wall SGW1 is due to the higher GFRP web reinforcement ratio, see Figure 4. For GFRP-RC walls, maximum reductions in residual drift ratios of 67.1%, 79%, and 80% were attained at 3.6% drift for walls GW1, GW2, and GW3, respectively, compared to the residual drift of the control wall (SW1). These results confirm that the minimal recorded residual deformation is due to the capability of self-centring behaviour of GFRP-RC walls.

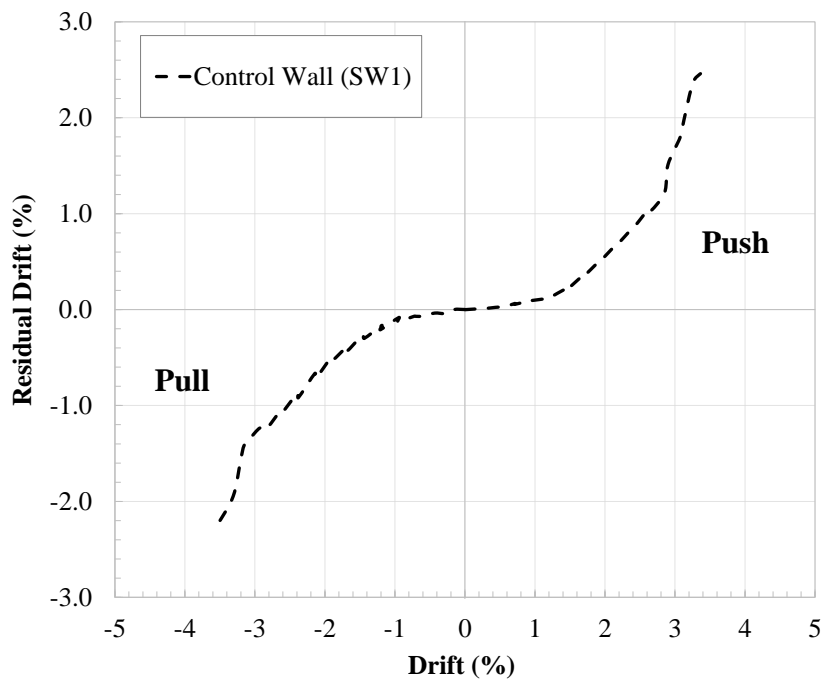


Figure 14 – Residual drift ratio of the steel-reinforced wall (SW1-control wall).

4.2. Energy dissipation and equivalent viscous damping

The dissipated energy during hysteresis (E_d) is given by the area enclosed by the hysteresis loop at each loading increment [24], as shown in Figure 16. The energy dissipated by each successive cycle was summed up to the energy of the previous cycles to calculate the cumulative energy dissipation. The results showed that lower energy dissipation was calculated for all walls in the early drift levels (lower than 1.0% drift) due to the lower occurred deformation of the tested walls to this drift level.

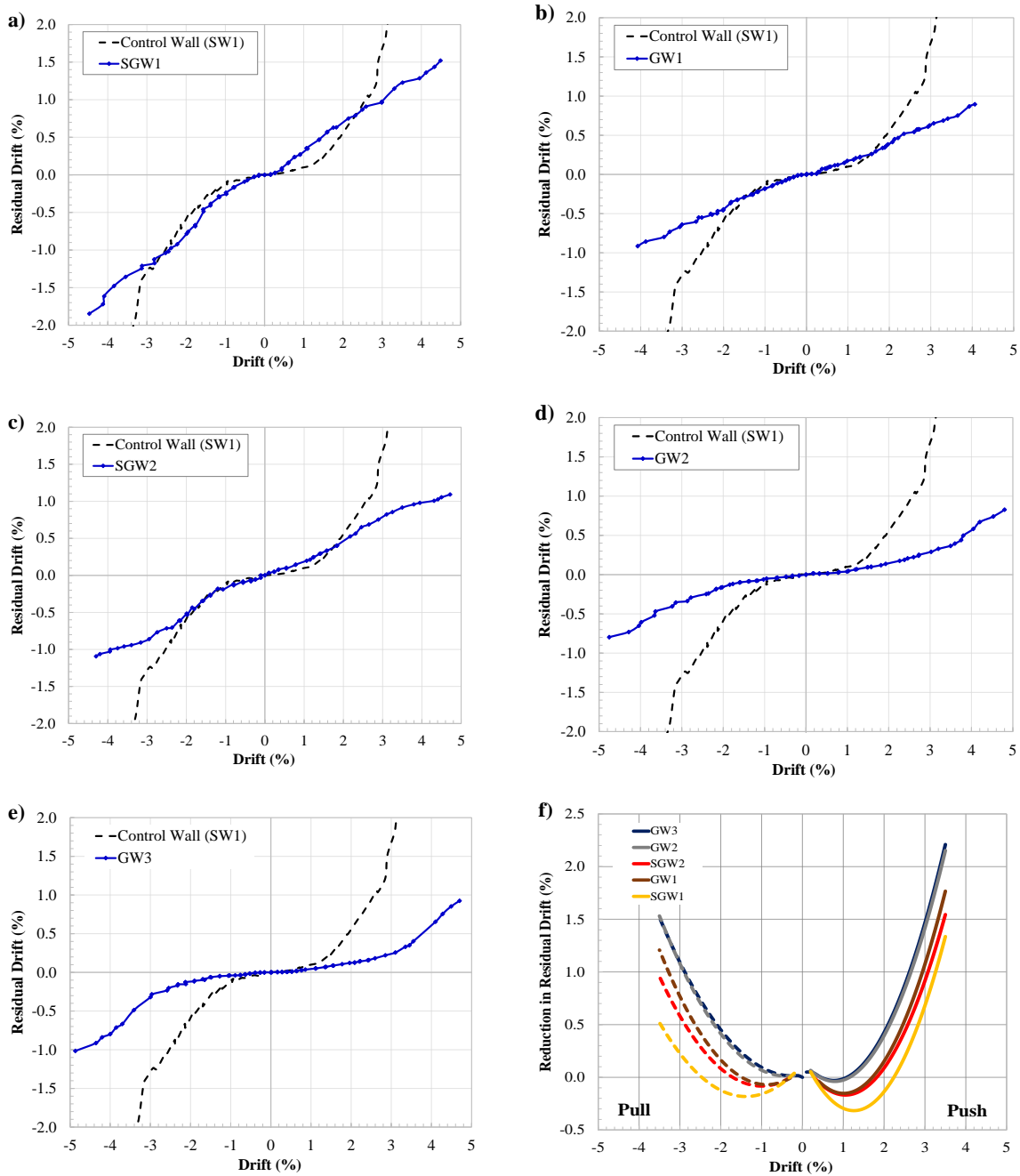


Figure 15 – Residual drift ratio of hybrid steel-GFRP walls (a&b), and GFRP-reinforced walls (c-e), and e) reduction in the residual drift ratios of hybrid walls with respect to control walls.

At higher drift levels, steel-reinforced wall (SW1) exhibited the most advantageous energy dissipation capacity (Figure 17). However, the dissipated energy of hybrid steel-GFRP reinforced walls exhibited a similar and considerable increase with the consecutive loading displacement due to the concentrated vertical steel rebar at the walls' sides. This increase in energy dissipation proved the favourable energy dissipation capacity of the hybrid steel-GFRP reinforced walls. Conversely, due to the elastic behaviour of GFRP bars, a lower energy dissipation rate is remarked in GFRP-reinforced walls.

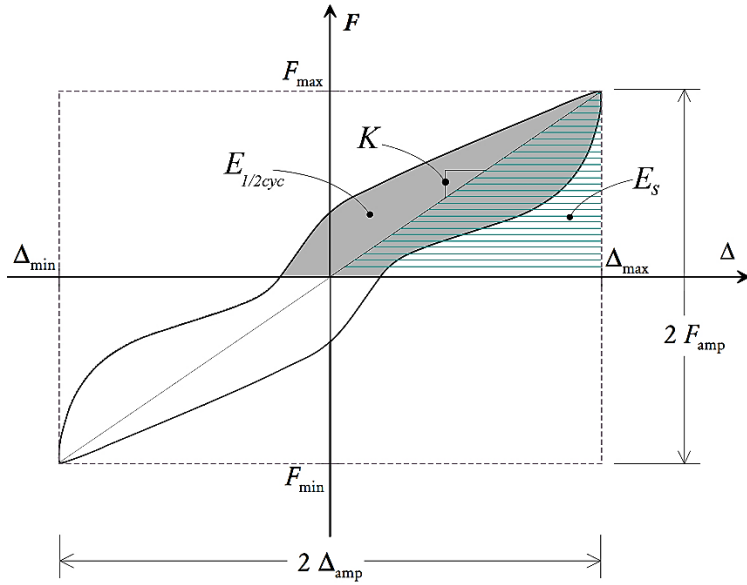


Figure 16 – Calculation of energy dissipation

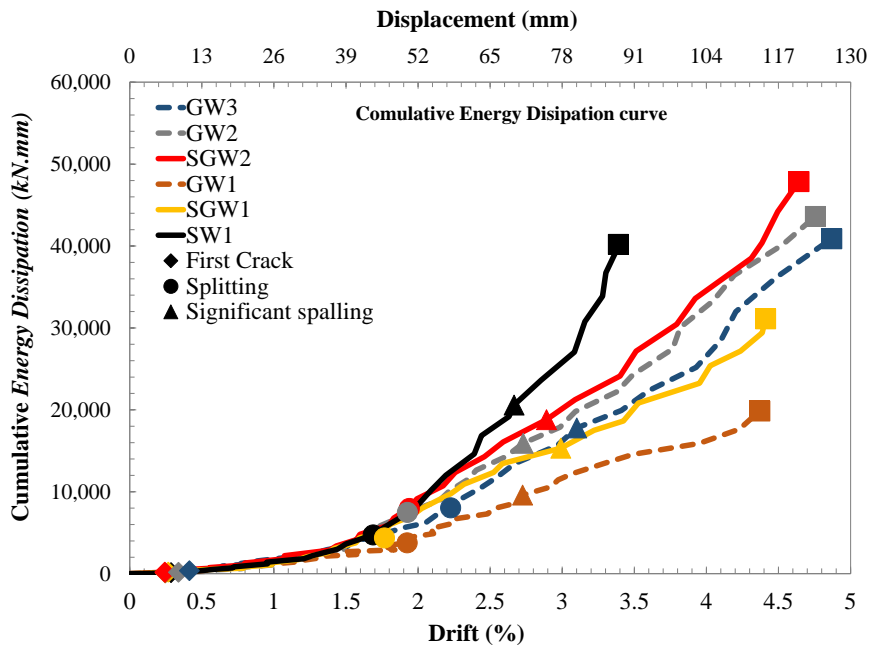


Figure 17 – Evolution of energy dissipation of tested walls

Additionally, the equivalent viscous damping ratio based on hysteresis, ξ_{hyst} , was used to evaluate the energy dissipation capacity of the shear wall. It was calculated using the area-based method according to the following equation:

$$\xi_{hyst} = \frac{1}{\pi} \frac{E_{1/2cyc}}{F_{amp} \cdot \Delta_{amp}} \quad \text{Eq. 6}$$

where $E_{1/2cyc}$ is the dissipated energy during the half-cycle. $E_s = F_{amp} \cdot \Delta_{amp}$ represents the elastic strain energy of the test wall that stored in an equivalent linear elastic system in one loading cycle. Figure 18 depicts the relationship between the equivalent viscous

damping ξ_{hyst} and the increase in the lateral drift ratios for all tested walls. In general, ξ_{hyst} tends to rise with an increase in drift ratio. Moreover, the obtained results showed that the steel-reinforced and hybrid steel-GFRP reinforced walls exhibited higher significantly equivalent viscous damping ratios compared to the GFRP-reinforced walls because of the plastic deformation of deformed steel bars. The equivalent viscous damping ratio reached 11.7% and 14.1% at the ultimate load and achieved 16.1% to 20.5% at the displacement of $2\Delta_u$ for hybrid steel-GFRP reinforced walls SGW1 and SGW2, respectively. By contrast, the GFRP-RC walls exhibited approximately 59%, 36%, and 35.8% reduction of ξ_{hyst} at ultimate load than that of the control steel-reinforced wall (SW1).

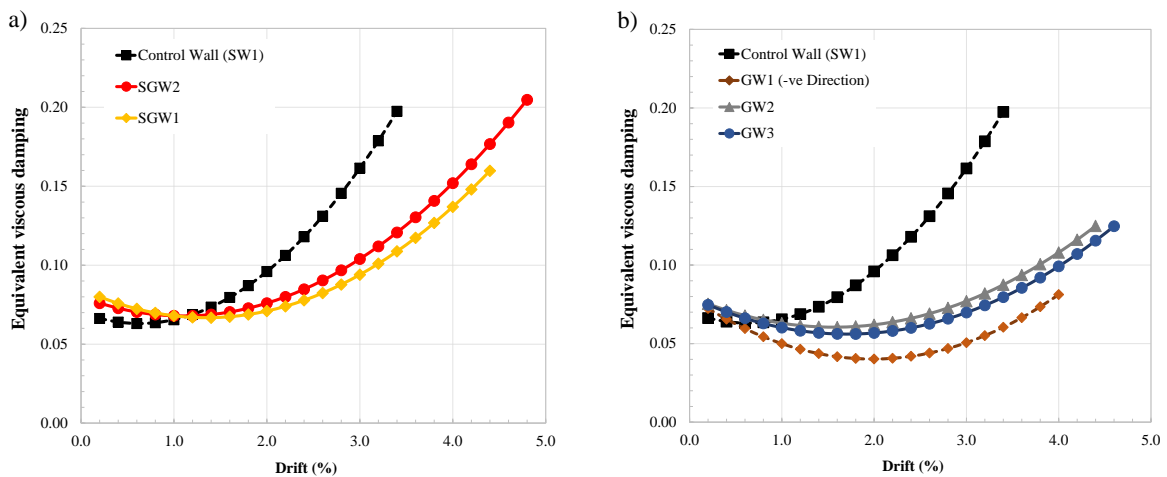


Figure 18 – Equivalent viscous damping coefficient: comparison between control steel-reinforced wall and a) hybrid steel-GFRP reinforced walls, b) GFRP-reinforced walls

4.3. Damage indices

Various damage indices were proposed in the literature [25, 26, 27, 28, 29], among others, in order to measure the resultant deficiencies and vulnerability of the structural members under seismic loading. Recently, various applications of damage indices were achieved based on loading history demand and capacity for estimating the damage and repair costs. Moreover, they are also utilized for decision-making in the post-earthquake evaluation and safety or vulnerability assessment for existing structures. Also, the performance levels of structural members can be evaluated at different drift levels using damage indices [30]. In general, the damage states were classified into the following five levels [28]:

$DI < 0.10$	No damage or minor local cracks
$0.10 \leq DI < 0.25$	Minor damage (e.g., light cracking throughout)
$0.25 \leq DI < 0.40$	Moderate damage (e.g., severe cracking local spalling)
$0.40 \leq DI < 1.0$	Sever damage (e.g., Concrete crushing and expose of bars)
$DI \geq 1.0$	Collapse

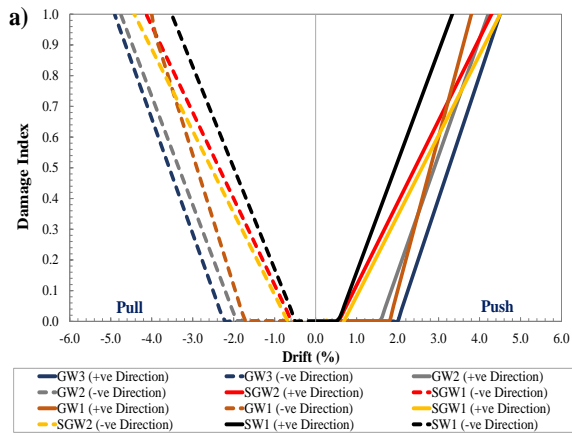
Following the approach found in the literature [30, 31], various damage indices for the tested walls were calculated to investigate the damage propagation and failure rate of all tested walls. Moreover, the resultant damage status in the hybrid steel-GFRP reinforced

walls and GFRP-RC walls were compared with the control steel-reinforced wall (SW1). Table 2 includes the formulation of adopted damage indices. Figure 19 depicts the damage indices based on displacement, dissipated energies, and effective stiffness, as well as the combined and performance indices, which were also plotted for all tested walls.

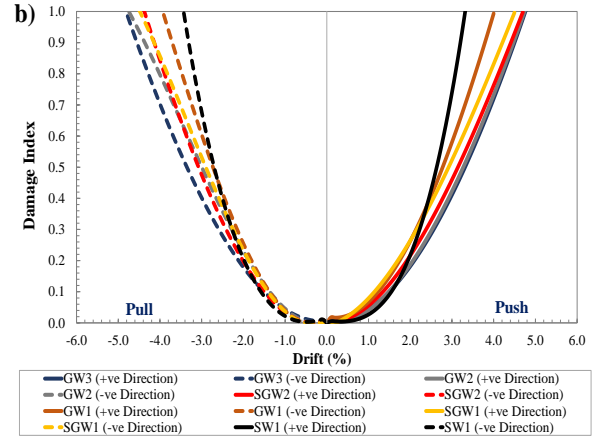
Table 2 - Different damage indices proposed by the researchers, [31, 30]

Damage index	Type	Formulation	Parameter Values
Powell & Allahabadi [25]	Based on the displacement	$DI = \frac{\Delta_m - \Delta_y (\sigma_r \Delta_\theta)}{\Delta_u - \Delta_y (\sigma_r \Delta_\theta)}$ $DI = \frac{\mu_m - 1}{\mu_u - 1}$	$\mu_u = \frac{\Delta_u}{\Delta_y (\sigma_r \Delta_\theta)}$ $\mu_m = \frac{\Delta_m}{\Delta_y (\sigma_r \Delta_\theta)}$
Rodriguez and Padilla [26]	Based on dissipated energy	$DI = \sum_{i=0}^n \frac{\int dE}{E}$	E = Energy dissipation
Kunnath & Jenne [27]	Based on effective Stiffness	$DI = 1 - \frac{K_m}{K_i}$	K_m = Secant stiffness K_i = Initial stiffness
Park and Ang [28]	Combined index	$DI = \frac{\Delta_m}{\Delta_u} + \beta \frac{\int dE}{F_y (\sigma_r \theta) \Delta_u}$	$\beta = 0.25$ $F_y (\sigma_r \theta)$ = Load at yielding for steel bars or spalling concrete for GFRP bars
Promis and Ferrier [29]	Performance index	$P = \frac{\sum E_m D_m}{\sum E_m}$	E_m = Dissipated energy D_m = Combined index in function of ductility and dissipated energy

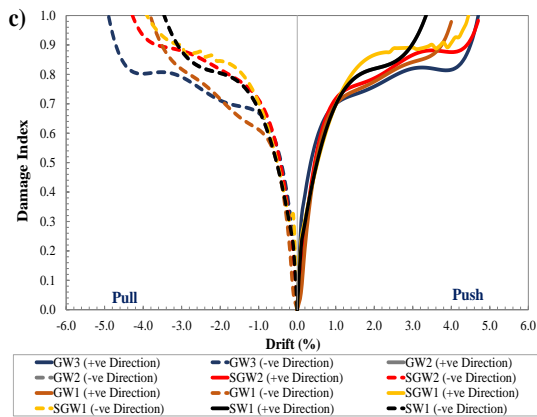
According to the results obtained from the damage index, based on the dissipated energy, the steel-reinforced wall (SW1) had lower damage than GFRP-reinforced walls at the early drift levels. However, a considerably higher damage rate was observed at the drift level corresponding to the yielding of steel bars. On the other hand, by analyzing the damage indices based on displacement energy and stiffness, the GFRP-RC walls experienced lower damage when compared with the steel-reinforced wall (SW1) at the same drift level as a result of its softer response with extensive concrete damage. Furthermore, the combined damage index also showed a more significant drift level of hybrid steel-GFRP, and GFRP reinforced walls with equal damage index compared to the control wall (SW1). This response of walls SGW1, SGW2, and walls GW1, GW2, and GW3 is mainly due to the low modulus of elasticity of GFRP bars, which allowed the walls to sustain higher deformation, at advanced loading levels, till failure. Moreover, by analyzing the performance index (Figure 19e), hybrid steel-GFRP and GFRP reinforced walls showed similar damage propagation where a lower damage rate was attained when compared with steel-reinforced wall at the same drift level.



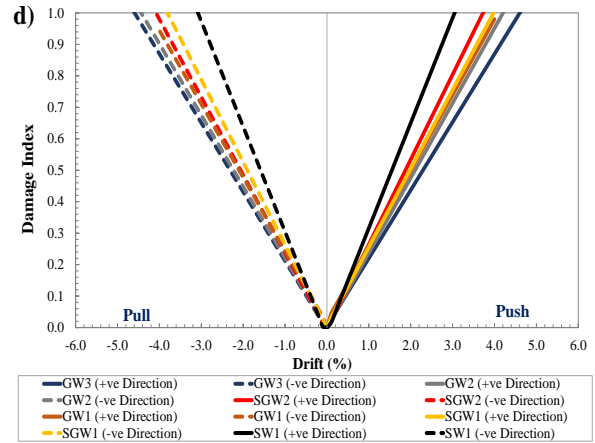
Linear damage index proposed by Powell and Allahabadi [25]



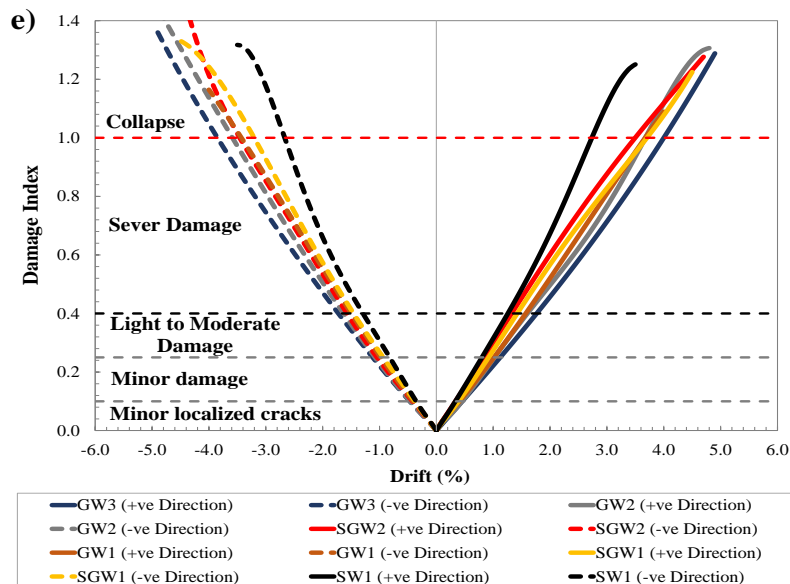
Damage index based on energy proposed by [26]



Damage index based on stiffness proposed by [27]



Combined damage index proposed by [28]



Performance index proposed by [29]

Figure 19 – Damaged indices of tested walls

5. Summary and conclusions

The current study was conducted on RC concrete shear walls to investigate the effectiveness of hybrid steel-GFRP system in reinforcing shear walls to withstand seismic loads. To accurately study the impact of the GFRP reinforcement ratio on the overall behaviour and self-centring performance of RC shear walls, several reinforcement ratios were selected for the hybrid steel-GFRP reinforced walls and for the GFRP-reinforced walls. The results are encouraging for the application of hybrid steel-GFRP reinforcement since the walls reached their maximum strength without exhibiting any signs of sliding shear failure, instability or anchorage failure. The permanent/plastic deformations in the concrete core are the source of the cumulative energy dissipation in GFRP-reinforced shear walls. Due to the elasticity of the GFRP reinforcement, all GFRP-reinforced walls exhibited relatively similar levels of energy dissipation at the same loading step. In addition, for hybrid steel-GFRP and GFRP-reinforced walls compared to the steel-reinforced wall, the elastic behaviour of GFRP bars led to lower damage rates with realigned cracks and recoverable deformation at the same drift level. Furthermore, increasing the GFRP-reinforcement ratio enhances the ultimate load capacity and significantly reduces crack width at moderate damage levels. Moreover, GFRP-RC walls showed stable hysteretic performance with a higher drift capacity than steel-reinforced walls.

- REFERENCES:

1. Z. Tuna, Seismic Performance, Modeling, and Failure Assessment of Reinforced Concrete Shear Wall Buildings, Los Angeles: PhD Thesis, University of California, 2012.
2. K. Beyer, A. Dazio et M. J. N. Priestley, «Quasi-Static Cyclic Tests of Two U-Shaped Reinforced Concrete Walls,» *Journal of Earthquake Engineering*, vol. 12, n° 17, pp. 1023-1053, 2008.
3. F. Talaei, Numerical Simulation and Economic Design of Concrete Shear Walls Reinforced with GFRP Bars, Alberta, Canada: M.Sc. Thesis, University of Alberta, 2017.
4. K. Orakcal, L. M. Massone et J. W. Wallace, «Shear Strength of Lightly Reinforced Wall Piers and Spandrels,» *ACI Structural Journal*, vol. 106, n° 14, pp. 455-465, 2009.
5. Y.-H. Oh, S. W. Han et L.-H. Lee, «Effect of boundary element details on the seismic deformation capacity of structural walls,» *Earthquake Engineering and Structural Dynamics*, vol. 31, n° 18, pp. 1583-1602, 2002.
6. M. Preti et E. Giuriani, «Ductility of a Structural Wall with Spread Rebars Tested in Full Scale,» *Journal of Earthquake Engineering*, vol. 15, n° 18, pp. 1238-1259, 2011.
7. L. M. Massone, K. Orakcal et J. W. Wallace, «Flexural and shear responses in slender RC shear walls,» *chez 13th World Conference on Earthquake Engineering*, Vancouver, B.C., Canada, 2004.

8. C. Kassem, A. S. Farghaly et B. Benmokrane, «Evaluation of Flexural Behavior and Serviceability Performance of Concrete Beams Reinforced with FRP Bars,» *Journal of Composites for Construction*, vol. 15, n° 15, pp. 682-695, 2011.
9. C. E. Bakis, L. C. Bank, V. L. Brown, E. Cosenza, J. F. Davalos, J. J. Lesko, A. Machida, S. H. Rizkalla et T. C. Triantafillou, «Fiber-Reinforced Polymer Composites for Construction—State-of-the-Art Review,» *Journal of Composites for Construction*, vol. 6, n° 12, pp. 73-87, 2002.
10. E. El-Salakawy, B. Benmokrane, A. El-Ragaby et D. Nadeau, «Field Investigation on the First Bridge Deck Slab Reinforced with Glass FRP Bars Constructed in Canada,» *Journal of Composites for Construction*, vol. 9, n° 16, pp. 470-479, 2005.
11. M. K. Sharbatdar et M. Saatcioglu, «Seismic Design of FRP Reinforced Concrete Structures,» *Asian Journal of Applied Sciences*, vol. 2, n° 13, pp. 211-222, 2009.
12. H. Tobbi, A. S. Farghaly et B. Benmokrane, «Concrete Columns Reinforced Longitudinally and Transversally with Glass Fiber-Reinforced Polymer Bars,» *ACI Structural Journal*, vol. 109, n° 14, pp. 551-558, 2012.
13. N. Mohamed, A. S. Farghaly, B. Benmokrane et K. W. Neale, «Flexure and Shear Deformation of GFRP-Reinforced Shear Walls,» *Journal of Composites for Construction*, vol. 18, n° 12, p. 04013044, 2014.
14. M. R. Ehsani, «Glass-fiber reinforcing bars,» chez *Alternative Materials for the Reinforcement and Prestressing of Concrete*, J. L. Clarke, Éd., New York, NY, E & FN & SPON, CRC Press, 1993, pp. 34-54.
 - A. Nanni, «Flexural Behavior and Design of RC Members Using FRP Reinforcement,» *Journal of Structural Engineering*, vol. 119, n° 11, pp. 3344-3359, 1993.
15. ACI 318, *Building code requirements for structural concrete and Commentary (ACI 318-19)*, Farmington Hills, MI: American Concrete Institute, 2019.
16. ACI 440.1R, *Guide for the design and construction of structural concrete reinforced with FRP bars*, Farmington Hills, MI: American Concrete Institute, 2015.
 - A. Hassanein, N. Mohamed, A. S. Farghaly et B. Benmokrane, «Effect of boundary element confinement configuration on the performance of GFRP-Reinforced concrete shear walls,» *Engineering Structures*, vol. 225, p. 111262, 2020.
17. ACI 440.1R-15, *Guide for the design and construction of structural concrete reinforced with FRP bars*, Farmington Hills, MI: American Concrete Institute, 2015.
18. T. Paulay et M. J. N. Priestley, *Seismic design of reinforced concrete and masonry buildings*, New York,: John Wiley and Sons Inc., 1995.
19. O. A. El-Azizy, M. T. Shedid, W. W. El-Dakhakhni et R. G. Drysdale, «Experimental evaluation of the seismic performance of reinforced concrete structural walls with different end configurations,» *Engineering Structures*, vol. 101, p. 246–263, 2015.

20. ASTM C39/C39M, «Standard test method for compressive strength of cylindrical concrete specimens,» American Society for Testing and Materials, West Conshohocken, PA, 2021.
21. FEMA 461, «Interim Testing Protocols for Determining the Seismic Performance Characteristics of Structural and Nonstructural Components,» Federal Emergency Management Agency, Redwood, CA , 2007.
 - A. K. Chopra, Dynamics of structures: Theory and applications to earthquake engineering, Englewood Cliffs, NJ: Prentice-Hall, Inc., 2000.
22. G. H. Powell et R. Allahabadi, «Seismic damage prediction by deterministic methods: concepts and procedures,» Earthquake Engineering and Structural Dynamics, vol. 16, n° 15, pp. 719-734, 1988.
23. M. E. Rodriguez et D. Padilla, «A damage index for the seismic analysis of reinforced concrete members,» Journal of Earthquake Engineering, vol. 13, n° 13, pp. 364-383, 2009.
24. S. K. Kunnath et C. Jenne, «Seismic damage assessment of inelastic RC structures,» chez 5th US national conference on earthquake engineering, EERI Chicago, Illinois, 1994.
25. Y.-J. Park, A. H.-S. Ang et Y. K. Wen, «Seismic damage analysis of reinforced concrete buildings,» Journal of Structural Engineering, vol. 111, n° 14, pp. 740-757, 1985.
26. G. Promis et E. Ferrier, «Performance indices to assess the efficiency of external FRP retrofitting of reinforced concrete short columns for seismic strengthening,» Construction and Building Materials, vol. 26, pp. 32-40, 2012.
27. M. Haji, H. Naderpour et A. Kheyroddin, «Experimental study on influence of proposed FRP-strengthening techniques on RC circular short columns considering different types of damage index,» Composite Structures, vol. 209, pp. 112-128, 2019.
28. S. M. Hosseini, M. Yekrangnia et A. V. Oskouei, «Effect of spiral transverse bars on structural behavior of concrete shear walls reinforced with GFRP bars,» Journal of Building Engineering, vol. 55, p. 104706, 2022.